ChemCatChem

Research Article
doi.org/10.1002/cctc.202201479

Chemistry Europe
European Chemical Societies Publishing

www.chemcatchem.org

$[Pd(2\text{-pymo})_2]_n/Al_2O_3$ as MOF Single Site Catalyst for the Selective Hydrogenation of Acetylene**

Sebastian Hock,[a] Martin Lucas,[a] Eva Kolle-Görgen,[a] Maximilian Mellin,[b] Jan P. Hofmann,[b] and Marcus Rose*[a]

Despite the great potential of metal-organic frameworks (MOFs) in catalysis, industrial applications are still scarce. This is mainly due to a lack of performance when changing from idealized lab conditions towards realistic conditions of the actual application. In this work, we demonstrate the applicability and outstanding catalytic performance of an alumina-supported $[Pd(2\text{-pymo})_2]_n$ MOF catalyst in the selective hydrogenation of acetylene to ethylene under industrial front-end conditions. It shows a competitive performance to an industrial benchmark catalyst and even exceeds it in terms of ethane selectivity due to the combination of well-defined isolated Pd active sites and synergies due to MOF-support-interactions. The high stability was proven for up to 60 h time-on-stream and supported by XPS and XRD structural analysis.

Introduction

Ethylene is one of the most important bulk platform chemicals with an annual global production of 214 million tons in 2021.[1] The industrially established primary production method is steam cracking of hydrocarbon feedstock, followed by separation and purification.[2–3] In the C_2 product stream after the de-ethanizer column it is necessary to reduce the acetylene content down to below 1 ppmv on the industrial scale by selective hydrogenation to ethylene.[3–4] Such an acetylene removal unit (ARU) can be integrated directly after the de-ethanizer, where the C_2-cut contains excess hydrogen and methane (*front-end*) or after the subsequent de-methanizer (*tail-end*).[2,5–6] Currently the *tail-end* process is more commonly applied as reaction control is more convenient due to control of the hydrogen/acetylene ratio. The high hydrogen fraction under *front-end* conditions can decrease the ethylene selectivity and increase the risk of hot spot formation or even reactor runaway and thus, renders the process control more challenging.[2–3,5,7–11] With a suitable catalyst and safe operations, the excess amount of hydrogen in the *front-end* integration is advantageous because then a higher conversion of acetylene as well as the suppression of oligo- and polymeric by-products ("green oil"/C_{4+} hydrocarbons) can be achieved.[2–3,5,7–11] Additionally, this reduces catalyst deactivation and results in a longer catalyst lifetime.[2–3,5,7–11] Furthermore, with the *front-end* method the removal and subsequent addition of hydrogen becomes obsolete because the hydrogen produced during steam cracking is used within a more efficient process integration.[2,5,12] For both process options the state-of-the-art catalysts are palladium/silver nanoparticles supported on alumina pellets.[4,8] However, due to the importance of the reaction, there has been a lot of research with focus on enhancing catalytic properties for palladium catalysts or even developing new catalysts.[2,4,11] Here metal-organic frameworks (MOFs) with their chemical versatility, high surface area and pore size variability, offer the possibility of directing selectivity and enhance the activity of the selective acetylene hydrogenation.[13–15] Recent studies on this reaction with specially designed MOFs for the separation of acetylene[16–21] and MOFs as catalysts, e.g. with open Fe^{III} sites,[22] show promising results. Research on palladium catalysts supported on MOF structures has also been in the focus with Pd supported on MOF-5,[23] Pd/UiO-67,[24] Pd@Mil-53[25] or Pd@ZIF-L.[26] To the best of our knowledge, no studies on acetylene hydrogenation with favourable Pd^{2+} nodes as part of a MOF itself have been reported, yet. $[Pd(2\text{-pymo})_2]_n$ (2-pymo = 2-pyrimidinolate) is the only currently known MOF using these kind of nodes and was first reported by Navarro et al.[27] Its catalytic performance has already been studied on the olefin hydrogenation of 1-octene and cyclodecene,[28–30] the oxidation of alcohols,[31–33] for the Suzuki-Miyaura cross-coupling reaction of arenediazonium tetrafluoroborate salts with arylboronic acids[34] and for phenylacetylene semi-hydrogenation in water.[18] The reported data show promising results especially for the selective catalytic hydrogenation but also the possibility of the reduction of Pd^{2+} to Pd^0 under reductive conditions, resulting in the collapse of the structure.[28–29] In this work, we explore the outstanding performance of the $[Pd(2\text{-pymo})_2]_n$ MOF for the selective catalytic hydrogenation of acetylene under industrially relevant reaction conditions. The advantages of defined isolated palladium sites[35–37] in a metal-organic-

[a] S. Hock, M. Lucas, E. Kolle-Görgen, Prof. Dr. M. Rose
Department of Chemistry, Chemical Technology
Technical University of Darmstadt
Alarich-Weiss-Str. 8, 64287 Darmstadt (Germany)
E-mail: marcus.rose@tu-darmstadt.de
[b] M. Mellin, Prof. Dr. J. P. Hofmann
Department of Materials and Earth Sciences, Surface Science Laboratory
Technical University of Darmstadt
Otto-Berndt-Str. 3, 64287 Darmstadt (Germany)

[**] *A previous version of this manuscript has been deposited on a preprint server (https://doi.org/10.26434/chemrxiv-2022-rx3hw).*

Supporting information for this article is available on the WWW under https://doi.org/10.1002/cctc.202201479

framework structure are proven. Additionally, we demonstrate how the stability and long-term catalytic performance can be significantly increased by supporting of the MOF particles and enabling a synergetic effect comparable to strong metal support interactions.

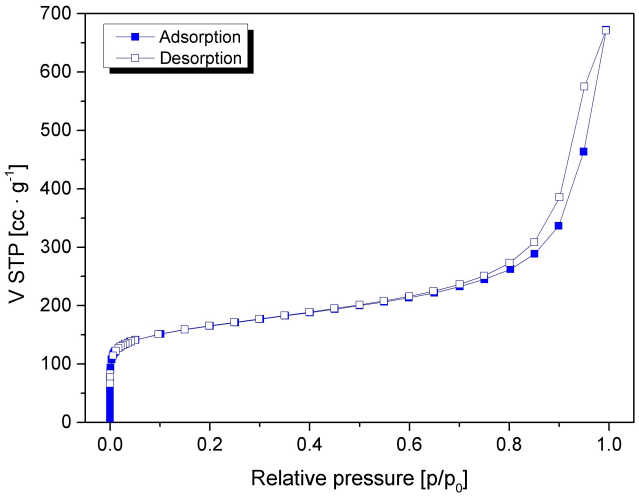

Figure 1. N_2 physisorption isotherm of pristine $[Pd(2\text{-pymo})_2]_n$ at 77 K.

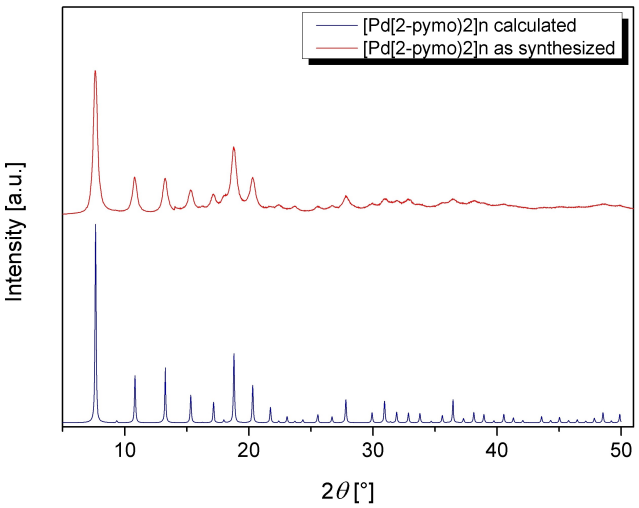

Figure 2. Powder X-ray diffractogram of $[Pd(2\text{-pymo})_2]_n$: calculated pattern (bottom) and $[Pd(2\text{-pymo})_2]_n$ as synthesized (top).

Results and Discussion

Synthesis and characterization of parental material

The synthesis of $[Pd(2\text{-pymo})_2]_n$ was carried out according to the previously reported route.[27–28] The resulting MOF occurs as a fine yellow powder. The quality of the material was characterized by N_2 physisorption and structural confirmation by XRD. From the measured isotherm (Figure 1) the BET specific surface area was determined in the relative pressure region $p/p_0 = 0.009–0.1$ to be 600 $m^2 g^{-1}$. Both the isotherm and the BET specific surface area precisely match the ones reported in literature[27] and thus, demonstrate a very robust and reproducible synthesis. The powder X-ray diffractogram (Figure 2) indicates an exact match between the calculated and the experimental patterns. Additionally, X-ray fluorescence measurements (SI Table S2) prove the expected composition. SEM and STEM images (Figure 3 and Figure S6) of the synthesized $[Pd(2\text{-pymo})_2]_n$ show uniform shapes, sizes and morphology of the particles.

Catalytic testing of $[Pd(2\text{-pymo})_2]_n$ in powder form

The as-synthesized $[Pd(2\text{-pymo})_2]_n$ powder was tested for its catalytic performance in the selective hydrogenation of acetylene under industrially relevant front-end conditions (Scheme 1 and Table 1). The applied reactor setup for fixed-bed catalyst testing under continuous gas feed conditions and online product analysis was recently reported by Hock et al.[10–11] For the experiments a typical feed composition of an acetylene removal unit (ARU) according to Gislason et al.[38] consisting of 39.00 mol% ethylene, 35.24 mol% methane, 25.00 mol% hydrogen, 0.40 mol% acetylene, 0.33 mol% propane (internal standard) and 250 ppm carbon monoxide was used (Table 1 #1).

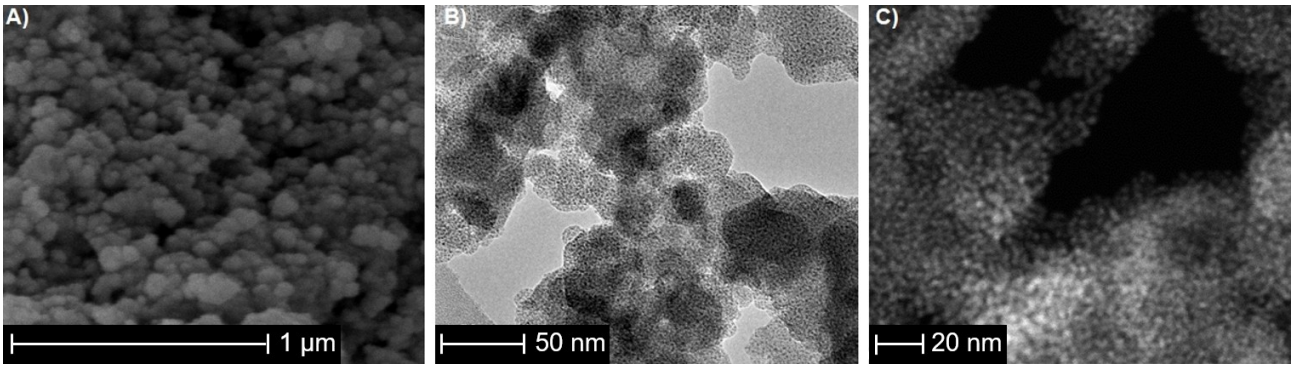

Figure 3. Electron microscopy of $[Pd(2\text{-pymo})_2]_n$: A) Scanning Electron Microscopy (SEM), B) Scanning Transmission Electron Microscopy (STEM), C) STEM dark field (DF). For different view and resolution see Figure S5.

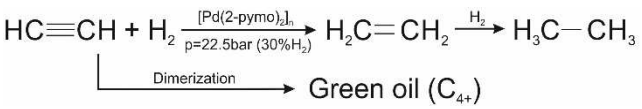

Scheme 1. Reaction scheme for the selective acetylene hydrogenation under industrial front-end conditions.

Table 1. Feed composition of the reported experiments.

Feed composition according to	#1 Gislason et al.[38]	#2 Hock et al.[10]
C_2H_4 [mol%]	39.00	37.00
H_2 [mol%]	25.00	35.56
CH_4 [mol%]	35.24	26.86
C_2H_2 [mol%]	0.40	0.30
C_3H_8 [mol%]	0.33	0.25
CO [ppm]	250	350

The experiments were carried out over a temperature range from 30–90 °C, which represents the industrially relevant range.[10] Starting at 30 °C in steps of 10 K, each temperature was analyzed over the course of 70 minutes reaching steady-state conditions. The temperature was then increased by steps of 10 K at a rate of 1 K·min^{-1} and the new conditions were monitored. The resulting acetylene conversion, ethane selectivity and C_4 selectivity of 250 mg $[Pd(2\text{-pymo})_2]_n$ as synthesized are shown in Figure 4. The numerical measurement data alongside the calculation and detailed information on 1 -butene, c-butene, t-butene and 1,3- butadiene formation is shown in the SI.

An increasing activity with increasing temperature is observed. At lower reaction temperatures the catalytic performance of $[Pd(2\text{-pymo})_2]_n$ in powder form is low, while at 70 °C however an acetylene conversion of 19.3% with a low ethane make of 0.010 mol% and a total C_4 selectivity of 8.4% was achieved. An increase of the reaction temperature to 90 °C more than doubled the conversion to 43.8% and decreased the

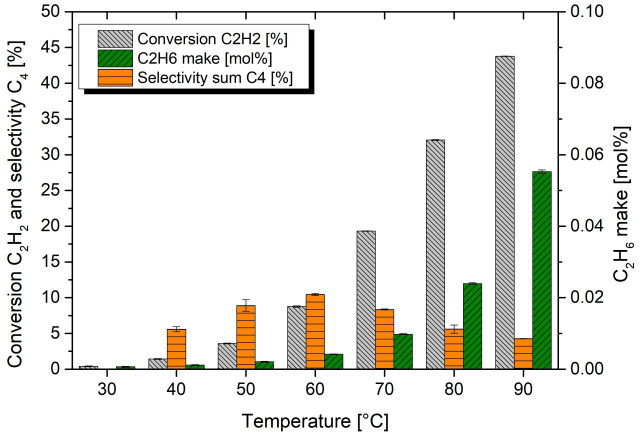

Figure 4. Reaction data of 250 mg $[Pd(2\text{-pymo})_2]_n$ as synthesized measured in a continuously operated fixed-bed reactor laboratory plant[11] using feed #1 (Table 1) with a volume flow of 62.7 L·h^{-1} (Table 1). The selectivity of 1-butene, c-butene, t-butene and 1,3- butadiene is summed up.

C_4 selectivity down to 4.2% due to the higher hydrogenation activity. As expected, the ethane make increased to 0.055 mol% due to a decreasing selectivity and over-hydrogenation. Overall, performance data of MOFs for a direct comparison have not been reported yet. A direct comparison with an industrial catalyst[10] shows a similar catalytic performance. A detailed analysis of the catalyst performance and properties (see XPS data in Figure 10) shows that a quantity of the Pd^{2+} was reduced to Pd^0 during the catalytic testing especially at elevated temperatures. N_2 physisorption reveals a decreased specific surface area. XRD analysis shows an amorphous diffractogram and XRF confirms a loss in the ratio of organic building blocks by evaluation of the Compton radiation. In summary, the *post-mortem* analysis after catalytic testing of the MOF powder shows signs of decomposition in the MOF structure under the applied reaction conditions. Yet, based on the very good initial catalytic performance further research focused on the improvement of the stability. Due to the highly exothermic nature of the acetylene hydrogenation reaction and the known thermal vulnerability of MOFs, the next logical step was the preparation and testing of supported $[Pd(2\text{-pymo})_2]_n/Al_2O_3$ catalysts in order to avoid hot spot formation by a high dispersion and aim for a temperature-gradient free catalytic performance.

Preparation and testing of $[Pd(2\text{-pymo})_2]_n/Al_2O_3$ catalysts

As suitable catalyst support alumina pellets were selected as they are typically applied with eggshell-supported Pd/Ag nanoparticles as active outer layer. Thus, in this work various methods for the immobilization of $[Pd(2\text{-pymo})_2]_n$ particles on alumina pellets were tested initially as there is basically no published knowledge on suitable binders for MOF particle shaping. Finally, a successful immobilization was obtained using minor amounts of methyl cellulose as binder (the detailed procedure is described in the SI).[39] With this method uniform $[Pd(2\text{-pymo})_2]_n/Al_2O_3$ catalyst pellets could be produced. The catalytic performance of samples with a weight loading of 1.13 wt% and 1.48 wt% of MOF with regard to the alumina support (weight of one Al_2O_3-pellet of 88.5 mg) are presented in this work. The selection is based on an initial screening (not shown) of four different loadings in the range of 0.2–1.8 wt%. As expected, the lowest loading exhibited a significantly reduced acetylene conversion. On the other hand, the highest loading did not give a further improvement in acetylene conversion which indicates the occurrence of mass transfer effects under the condition of substrate limitation. The eggshell catalyst pellets were tested in a modified laboratory plant suitable for catalyst pellets aligned within four TEMKIN reactor modules (Figure 5) as reported recently.[10]

For the catalytic testing the same program and temperature ramp as for the previous powder experiments were used, but this time 11 pellets of $[Pd(2\text{-pymo})_2]_n/Al_2O_3$ were tested using the same feed composition #1 (Table 1). The results (Figure 6) already show a high conversion of acetylene at lower temperatures with 82.8% at 70 °C and reaching full conversion at 80 °C.

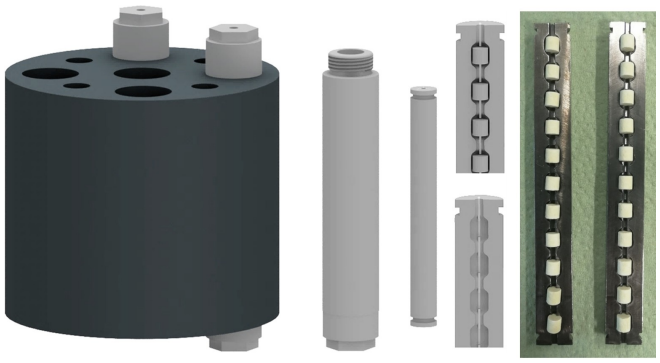

Figure 5. From left to right: heating block for up to four reactor tubes; detailed view of a reactor tube; closed TEMKIN module consisting of two half shells; schematic display of a half shell with one place holder packed with catalyst pellet and empty; photograph of prepared $[Pd(2\text{-}pymo)_2]_n/Al_2O_3$ catalyst pellets fitted in the two TEMKIN modules.

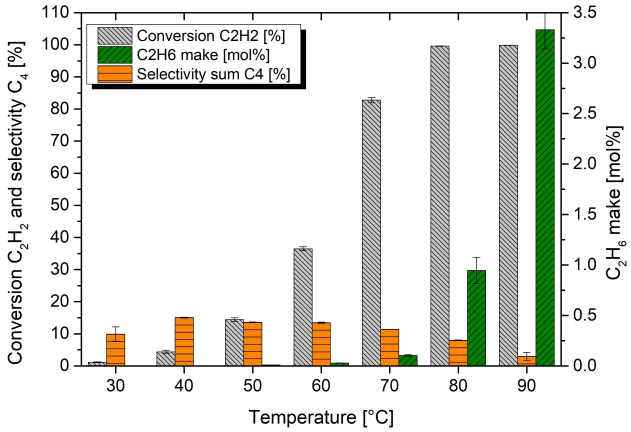

Figure 6. Reaction performance of 11 pellets of prepared eggshell catalyst with a weight loading of 1.13 wt% $[Pd(2\text{-}pymo)_2]_n$, tested under a volume flow of 12.9 $L \cdot h^{-1}$ of feed #1 (Table 1).

Up to the full conversion the ethane make is low with 0.103 mol% at 70 °C but strongly increases at 80 °C to 0.947 mol%. A further increase of the reaction temperature to 90 °C leads to an ethane make of 3.331 mol%, at which point more ethylene than acetylene is converted and indicates runaway conditions. The total sum of the C_4 selectivity amounts up to 10.4% at 70 °C and only 7.8% at full conversion at 80 °C. Especially at 70 °C the reported catalytic data of the $[Pd(2\text{-}pymo)_2]_n/Al_2O_3$ catalyst is outstanding with very high and selective conversion of acetylene.

In our previous work,[10] we reported the catalytic performance of 22 pellets of an industrial Pd–Ag/Al_2O_3 acetylene hydrogenation catalyst. For an ideal comparison to the industrial benchmark we therefore prepared 22 pellets of the $[Pd(2\text{-}pymo)_2]_n/Al_2O_3$ eggshell catalyst in the same cylindrical modification and a weight loading of 1.48 wt% of MOF with regard to the alumina support. These 22 catalyst pellets were then measured under the same feed composition #2 (Table 1), pressure, volume flow and in the same reactor setup as the industrial benchmark in the previous work.[10–11] The comparison (Figure 7) shows a similar behavior of the two catalysts at 90 °C, with both at full conversion and an ethane make of 0.37 mol%. But at 80 °C the ethane make of the $[Pd(2\text{-}pymo)_2]_n/Al_2O_3$ catalyst is with 0.054 mol% significantly lower than the industrial Pd–Ag/Al_2O_3 catalyst with 0.144 mol% under comparable conversion. The ethane make of $[Pd(2\text{-}pymo)_2]_n/Al_2O_3$ catalyst at lower temperatures is also better than the industrial benchmark but here the conversion of the industrial Pd–Ag/Al_2O_3 catalyst excels that of the presented catalyst. Also, the combined C_4 selectivity of the industrial benchmark catalyst is lower over the temperature program. Overall, the $[Pd(2\text{-}pymo)_2]_n/Al_2O_3$ catalyst shows a very similar catalytic performance compared to the industrial benchmark catalyst. Moreover, in its current form, a reduction of more than 62% of ethane make at 80 °C with only 5.4% less acetylene conversion is remarkable. This observation might indicate a pore size selectivity of the MOF catalysts as acetylene (van der Waals dimensions: 3.4 Å to 5.7 Å)[40] is slender than ethylene (van der Waals dimensions: 4.3 Å to 4.8 Å)[40] with a $[Pd(2\text{-}pymo)_2]_n$-MOF pore opening of 4.8 Å.[27]

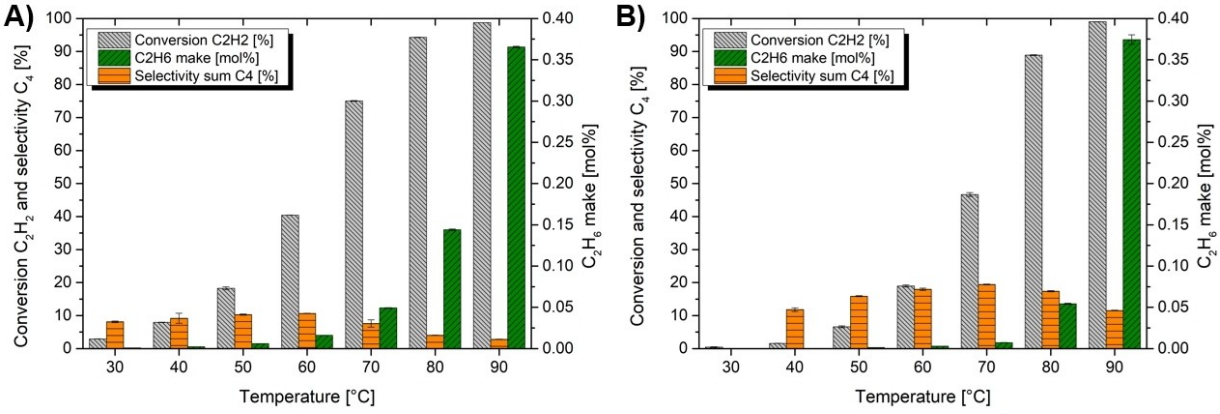

Figure 7. A) Comparison of the catalytic behavior of 22 pellets of the industrial catalyst (see previous work[10] Figure 4.b) and B) 22 pellets of the prepared eggshell catalyst with a weight loading of 1.48 wt% $[Pd(2\text{-}pymo)_2]_n$, both under the same reaction conditions and a volume flow of 62.7 $L \cdot h^{-1}$ of feed #2 (Table 1).

As a follow-up to the benchmark experiment a long-time study of the catalyst performance at 70 °C under a volume flow of 62.7 $L \cdot h^{-1}$ of feed #2 (Table 1) was carried out. The acetylene conversion, ethane make and the C_4 selectivity were monitored over the course of 50 h as shown in Figure 8. The detailed formation of 1-butene, c-butene, t-butene and 1,3- butadiene was also tracked (Figure S4). Over the total 50 h time-on-stream the $[Pd(2\text{-pymo})_2]_n/Al_2O_3$ eggshell catalyst showed a very stable performance (Figure 8). The acetylene conversion dropped only slightly from 47.5 % at the beginning to 44.9 % at the end. The ethane make remained low, with only a slight increase from 0.008 mol % to 0.010 mol %. The most significant observation was the reduction of the C_4 selectivity from 18.7 % at the start to 14.6 % at the end of the 50 h period. The detailed analysis of the C_4 species formation (Figure S4) revealed a reduction of 1-butene, c-butene and t-butene selectivity over the course of the experiment. Only the formation of 1,3-butadiene remained rather constant. In summary, the catalytic performance of the $[Pd(2\text{-pymo})_2]_n/Al_2O_3$ eggshell catalyst at a total time on stream of 60 h remained competitive to the industrially applied benchmark catalyst.

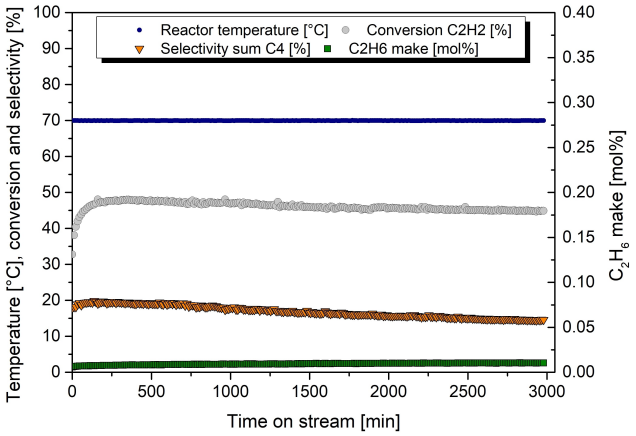

Figure 8. 22 pellets of prepared eggshell catalyst with a weight loading of 1.48 wt % $[Pd(2\text{-pymo})_2]_n$, tested for 50 h at 70 °C under 62.7 $L \cdot h^{-1}$ of feed #2 (Table 1).

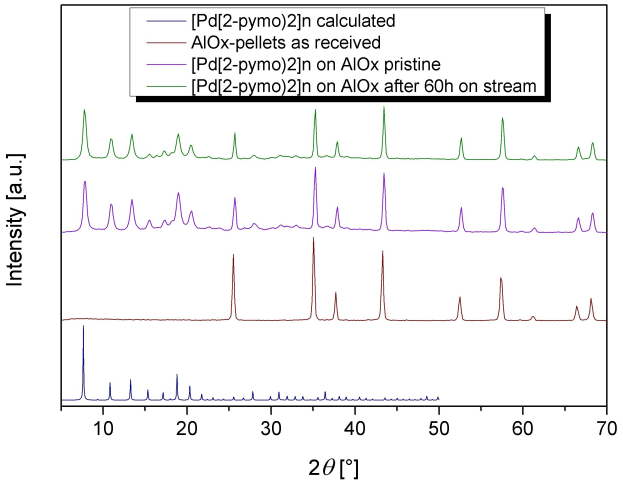

Figure 9. X-ray diffraction pattern of the egg-shell $[Pd(2\text{-pymo})_2]_n$ before and after catalysis with the calculated egg-shell $[Pd(2\text{-pymo})_2]_n$ and the measured Al_2O_3 support as reference.

Post mortem analysis of $[Pd(2\text{-pymo})_2]_n/Al_2O_3$ catalyst

A post mortem characterization of the catalyst pellets after the benchmark experiment (Figure 7 B) and long time-on-stream experiments (Figure 8) was carried out using XRD for the bulk structure as well as X-ray photoelectron spectroscopy (XPS) to gain information on the oxidation state of the MOF-incorporated Pd. In Figure 9 a comparison between the calculated $[Pd(2\text{-pymo})_2]_n$ XRD pattern, the pure measured Al_2O_3 support, egg-shell $[Pd(2\text{-pymo})_2]_n/Al_2O_3$ as prepared and the egg-shell $[Pd(2\text{-pymo})_2]_n/Al_2O_3$ after 60 h time-on-stream is displayed. Besides a minor loss in intensity, no changes of the X-ray diffraction pattern of the pristine and the used egg-shell $[Pd(2\text{-pymo})_2]_n$ catalyst could be observed.

Furthermore, the catalyst was analyzed by XPS as the Pd^{2+} ions as nodes are necessary for the integrity of the metal-organic-framework structure. The binding energies of the two discernible spectra components in the Pd 3d detail spectra (Figure 10) indicate palladium in the oxidation state 2 + /oxide form and to a small extent in the metallic state.[41–42] It can be concluded that for powders as well as pellets the 2 + oxidation state is maintained after catalysis. The ratio Pd^0/Pd^{2+} changed from 0.13 in pristine to 0.29 after a total of 8 h time-on-stream of the powder. In contrast, for the pellets, after several experiments and a total time-on-stream of 60 h, the ratio changed only slightly from 0.09 in pristine to 0.11.

The XRD and XPS post-mortem analysis in summary shows a vast improvement in the durability of the eggshell catalysts under reaction conditions. With $[Pd(2\text{-pymo})_2]_n$ immobilized on Al_2O_3 pellets, the Pd^{2+} nodes, which are vital for the integrity of the MOF structure, stay intact even after 60 h time-on-stream, while as-synthesized powder $[Pd(2\text{-pymo})_2]_n$ showed an increase of metallic Pd^0 of 223 % after only 8 h time-on-stream. Hence, a high dispersion of the supported MOF particles stabilized by a binder enables a significant stabilization regarding the reduction behavior and hence, drastically improves the overall stability.

The nature of the actual active sites can be concluded from the observed behavior and additional CO chemisorption data (Table S3). It is obvious that upon reduction and nanoparticle formation at higher temperatures the activity decreases as less Pd is accessible due to a decreasing dispersion. This clearly indicates active sites based on the MOF framework structure. From the ideal MOF structure it is conceivable that the tetrahedrally coordinated Pd^{2+} is coordinatively saturated and sterically hindered and might, thus, not be an available active site. However, structural defects in the microcrystalline MOF and especially terminating Pd-ions at the crystallite edges and the external surface area of the particle are very likely coordinatively unsaturated and sterically accessible. CO chemisorption exhibits that 9.9 mol-% of the contained Pd is available for CO adsorption. Hence, these sites are very likely

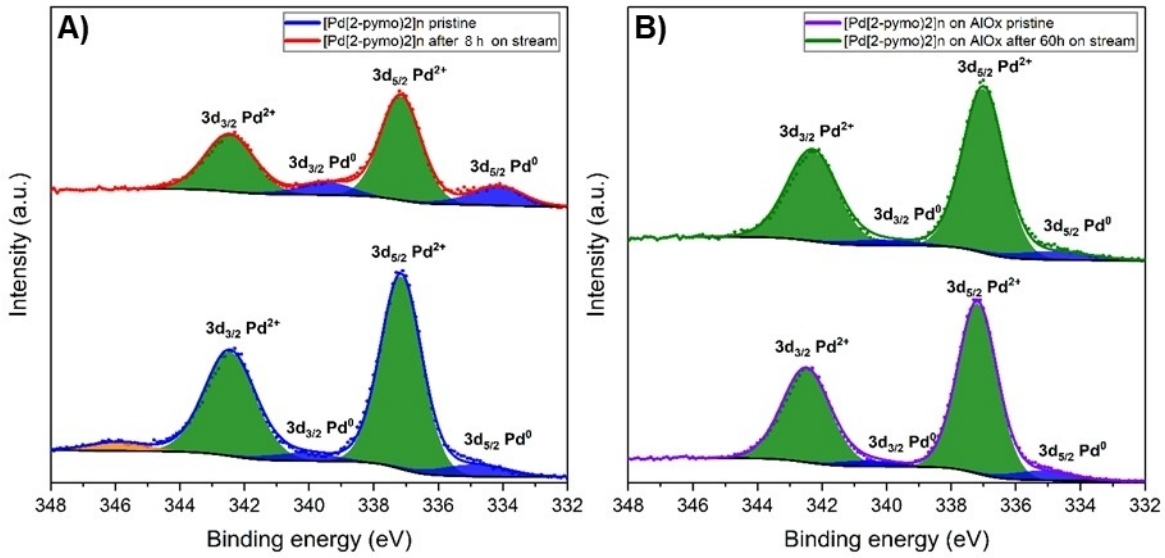

Figure 10. A) XPS detail spectra of palladium 3d pattern of the powdered $[Pd(2\text{-pymo})_2]_n$ in pristine state (bottom) and after 8 h time on stream (top) as well as for B) egg-shell $[Pd(2\text{-pymo})_2]_n$ on Al_2O_3 support in pristine state (bottom) and after 60 h time on stream (top).

also suitable hydrogenation sites of the MOF framework structure. Overall, this demonstrates that a targeted defect/surface engineering of such MOFs could be used to specifically tune the catalytic performance as single atom catalysts.

Conclusion

In this work, the outstanding catalytic performance in the selective hydrogenation of acetylene of $[Pd(2\text{-pymo})_2]_n$ MOF under industrial *front-end* conditions was reported. The decomposition of the MOF structure could be prevented by the immobilization on Al_2O_3 pellets. Also, the preparation of $[Pd(2\text{-pymo})_2]_n/Al_2O_3$ eggshell catalysts vastly increased the catalytic performance, which is comparable to an industrial benchmark catalyst and even exceeds it in terms of ethane make. XPS and XRD analysis revealed a high catalyst stability even after 60 h time-on-stream at competitive performance. Based on the experimental evidence the actual active sites are most likely coordinatively unsaturated Pd ions of the framework structure within defects and at the edges of the MOF crystallites and particles. Overall, the great potential of MOFs as single site catalysts is proven for this specific application and future work should emphasize industrially relevant reaction conditions especially taking into account stability and the performance for longer times-on-stream.

Experimental Section

Materials

Hydrogen (H_2, N5.0), a hydrogen/carbon monoxide mixture (0.15 mol% of CO, N18; remainder H_2, N3.0), methane (CH_4, N2.5), ethylene (C_2H_4, N3.5), an acetylene mixture (1.2 mol% of C_2H_2, N2.6; 1 mol% of C_3H_8, N2.5; remainder CH_4, N2.5), and argon (Ar, N5.0) were obtained from Air Liquide. Potassium tetrachloropalladate (K_2PdCl_4, 98%), 2-hydroxypyrimidine hydrochloride ($C_4H_4N_2O\cdot HCl$, 98%), sodium hydroxide (NaOH, 98%) and methylcellulose (CAS 9004-67-5) were purchased from Sigma Aldrich. Cylindrical Al_2O_3 pellets (4.5 mm × 4.5 mm) were obtained from ORI Catalyst Leuna GmbH. All chemicals were used as received.

Synthesis of $[Pd(2\text{-pymo})_2]_n$

The synthesis of the MOF $[Pd(2\text{-pymo})_2]_n$ was prepared according to published procedure.[27–28] An aqueous solution of potassium tetrachloropalladate (K_2PdCl_4, 7.7 mmol) was mixed with an aqueous solution of 2-hydroxypyrimidine hydrochloride ($C_4H_4N_2O\cdot HCl$, 15.4 mmol) and stirred for 4 h at room temperature. The precipitate trans-$[PdCl_2(2\text{-Hpymo})_2]$ was filtered off, washed and suspended in water. Afterwards, sodium hydroxide (NaOH, 7.7 mmol) was added and the suspension was refluxed for 48 h. The filtered solid was dried under reduced atmosphere and thus the MOF $[Pd(2\text{-pymo})_2]_n$ was obtained.

Preparation of egg-shell catalyst

For the support cylindrical α-Al_2O_3 pellets with a diameter of 4.5 mm and height of 4.5 mm were used. For the immobilization of the active component on the support a dip-coating method was used. Therefore, a stock solution consisting of methyl cellulose and water in a ratio of 1 to 1000 was prepared. $[Pd(2\text{-pymo})_2]_n$ was added to this stock solution in a ratio of 1 to 20 or 1 to 30. The Al_2O_3 pellets were dipped in the resulting suspension and dried at 80 °C. The dip-coating and drying process was repeated three times.

Selective hydrogenation of acetylene

The detailed experimental setup for the powder reactor was published by Hock et al.[11] and the details of TEMKIN setup were

shown by Hock et al.[43] The feed compositions specified in Table 1 manuscript were created by adding the gas mixtures listed in *MATERIALS* over the mass flow controller network. The composition of the outlet streams was continuously measured via gas chromatography (Shimadzu GC 2010 Plus with RT-Alumina BOND/MAPD column; 30 m; ID 0.53 mm; film thickness 10 μm; carrier gas helium) every 11 minutes with an FID analyzer. Before each experiment the exact feed composition was analyzed over a bypass measurement for at least 60 minutes. In each experiment, the temperatures 30, 40, 50, 60, 70, 80 and 90 °C were measured for 70 minutes. In between, the temperature was ramped at 1 °C · min^{-1}.

X-Ray powder diffraction and energy dispersive X-ray fluorescence

The X-ray powder diffraction data were obtained at room temperature by using a Bruker D2 Phaser diffractometer. For the destruction free analysis of the catalyst pellets a special sample holder was designed and used.

For the XRF measurements a "Epsilon4" from PANalytical was used.

Physisorption

Nitrogen physisorption measurements were carried out with an "Autosorb iQ" from Quantachrome Instruments. The pre-dried samples were degassed under vacuum at 200 °C for 20 h. The BET specific surface area was determined in the relative pressure region $p/p_0 = 0.05–0.25$.

Electron microscopy

SEM images were taken on a HREM XL 30 FEG from Philips with 10 keV and detection of the secondary electrons. For a sufficient conductivity the samples were sputtered with gold with 30 mA for 120 s.

A scanning transmission electron microscope (ZEISS CrossBeam 350, EHT 30 kV) was used for characterization of the morphology of the nanoparticles. The system has STEM-in-SEM capabilities, which can provide bright field (BF), dark field (DF) as well as a high angle annular dark field (HAADF) STEM imaging capability.

XPS

All experiments were performed in the DAISY-Bat vacuum-cluster tool (Darmstadt Integrated System for Battery Research, ULVAC-PHI VersaProbe II) with a base pressure in the analysis chamber below $5 \cdot 10^{-9}$ mbar. Monochromatized Al K_α radiation (1486.7 eV) was provided by standard laboratory excitation sources set at 1.69 mA and 15 kV with a spot size of 200 μm. The machine is periodically calibrated for having a Fermi edge of a clean silver foil at 0 eV. Powders were pressed into indium foil and pellets were cut and scratched on the backside to obtain thin samples. Due to strong charging effects, an electron flood gun was used in every measurement.

All detail spectra were measured by applying a pass energy of 23.5 eV and a step size of 0.1 eV. The backgrounds of the acquired spectra were subtracted using the Shirley method.[44] Ratio were determined by fitting the peak areas of the $3d_{5/2}$ Peaks in CasaXPS (version 2.3.25rev1.0P).[45] The areas were then corrected by a self-measured transmission function, EAL (effective attenuation length)[46] as well as Scofield magic angle corrected cross sections.[44]

For fitting the Pd 3d peaks, the GL(30) line shape was used for the oxide component and an asymmetric pseudo-Voigt function referred to as LF(0.76,1.5,55,300) line shape was used for the metallic component.[47] For both $3d_{3/2}$ peaks, an area constraint of 2/3 with respect to the $3d_{5/2}$ were used. An additional FWHM constraint for the $3d_{3/2}$ metal peaks was used. A position constraint for $3d_{3/2}$ of 5.3 eV was used additionally, which represents the typical spin-orbit splitting energy for Pd metal as well as for the oxides.[41–42]

Acknowledgements

The work was inspired by and carried out within the preparation of the recently granted collaborative research center "Iron, upgraded!" (CRC 1487) funded by the German Research Foundation (DFG, project number 443703006). Open Access funding enabled and organized by Projekt DEAL.

Conflict of Interest

The authors declare no conflict of interest.

Data Availability Statement

The data that support the findings of this study are available from the corresponding author upon reasonable request.

Keywords: heterogeneous catalysis · hydrogenation · industrial chemistry · metal-organic-framework · selective acetylene hydrogenation · supported catalysts

[1] https://www.statista.com/statistics/1067372/global-ethylene-production-capacity/ (18.11.2022).
[2] A. J. McCue, J. A. Anderson, *Front. Chem. Sci. Eng.* **2015**, *9*, 142–153.
[3] A. Pachulski, R. Schödel, P. Claus, *Appl. Catal. A* **2012**, *445*, 107–120.
[4] M. T. Ravanchi, S. Sahebdelfar, S. Komeili, *Rev. Chem. Eng.* **2018**, *34*, 215–237.
[5] A. Borodziński, G. C. Bond, *Catal. Rev.* **2006**, *48*, 91–144.
[6] M. R. Ball, K. R. Rivera-Dones, E. B. Gilcher, S. F. Ausman, C. W. Hullfish, E. A. Lebrón, J. A. Dumesic, *ACS Catal.* **2020**, *10*, 8567–8581.
[7] M. Kuhn, M. Lucas, P. Claus, *Chem. Eng. Technol.* **2015**, *38*, 61–67.
[8] M. Kuhn, M. Lucas, P. Claus, *Ind. Eng. Chem. Res.* **2015**, *54*, 6683–6691.
[9] M. Kuhn, M. Lucas, P. Claus, *Catal. Commun.* **2015**, *72*, 170–173.
[10] S. Hock, L. Iser, M. Lucas, M. Rose, *Chem. Ing. Tech.* **2022**, *94*, 1704–1710.
[11] S. Hock, C. V. Reichel, A.-M. Zieschang, B. Albert, M. Rose, *ACS Sustainable Chem. Eng.* **2021**, *9*, 16570–16576.
[12] Q. Zhang, Y. Xu, Q. Wang, W. Huang, J. Zhou, Y. Jiang, H. Xu, L. Guo, P. Zhang, J. Zhao, *Chem. Commun.* **2019**, *55*, 14910–14913.
[13] G. Bauer, D. Ongari, D. Tiana, P. Gäumann, T. Rohrbach, G. Pareras, M. Tarik, B. Smit, M. Ranocchiari, *Nat. Commun.* **2020**, *11*, 1059.
[14] M. E. Davis, *Nature* **2002**, *417*, 813.
[15] M. Zhao, K. Yuan, Y. Wang, G. Li, J. Guo, L. Gu, W. Hu, H. Zhao, Z. Tang, *Nature* **2016**, *539*, 76–80.
[16] T.-L. Hu, H. Wang, B. Li, R. Krishna, H. Wu, W. Zhou, Y. Zhao, Y. Han, X. Wang, W. Zhu, *Nat. Commun.* **2015**, *6*, 1–9.
[17] Y. Liu, B. Wang, Q. Fu, W. Liu, Y. Wang, L. Gu, D. Wang, Y. Li, *Angew. Chem. Int. Ed.* **2021**, *60*, 22522–22528; *Angew. Chem.* **2021**, *133*, 22696–22702.

[18] A. W. Augustyniak, A. M. Trzeciak, *ChemCatChem* **2021**, *13*, 2145–2151.
[19] X. Zhang, Y. Yang, X. Lv, Y. Wang, L. Cui, *Catalysts* **2017**, *7*, 382.
[20] Z. Zhang, S. B. Peh, Y. Wang, C. Kang, W. Fan, D. Zhao, *Angew. Chem. Int. Ed.* **2020**, *59*, 18927–18932; *Angew. Chem.* **2020**, *132*, 19089–19094.
[21] S.-C. Xiang, Z. Zhang, C.-G. Zhao, K. Hong, X. Zhao, D.-R. Ding, M.-H. Xie, C.-D. Wu, M. C. Das, R. Gill, *Nat. Commun.* **2011**, *2*, 1–7.
[22] M. a. Tejeda-Serrano, M. Mon, B. Ross, F. Gonell, J. s. Ferrando-Soria, A. Corma, A. Leyva-Pérez, D. Armentano, E. Pardo, *J. Am. Chem. Soc.* **2018**, *140*, 8827–8832.
[23] S. Opelt, S. Türk, E. Dietzsch, A. Henschel, S. Kaskel, E. Klemm, *Catal. Commun.* **2008**, *9*, 1286–1290.
[24] K. Choe, F. Zheng, H. Wang, Y. Yuan, W. Zhao, G. Xue, X. Qiu, M. Ri, X. Shi, Y. Wang, *Angew. Chem.* **2020**, *132*, 3679–3686; *Angew. Chem. Int. Ed.* **2020**, *59*, 3650–3657.
[25] X. Li, L. Song, D. Gao, B. Kang, H. Zhao, C. Li, X. Hu, G. Chen, *Chem. Eur. J.* **2020**, *26*, 4419–4424.
[26] S. Xue, H. Jiang, Z. Zhong, Z.-X. Low, R. Chen, W. Xing, *Microporous Mesoporous Mater.* **2016**, *221*, 220–227.
[27] J. A. Navarro, E. Barea, J. M. Salas, N. Masciocchi, S. Galli, A. Sironi, C. O. Ania, J. B. Parra, *Inorg. Chem.* **2006**, *45*, 2397–2399.
[28] S. Opelt, V. Krug, J. Sonntag, M. Hunger, E. Klemm, *Microporous Mesoporous Mater.* **2012**, *147*, 327–333.
[29] S. Schuster, E. Klemm, M. Bauer, *Chem. Eur. J.* **2012**, *18*, 15831–15837.
[30] F. X. L. i Xamena, A. Abad, A. Corma, H. Garcia, *J. Catal.* **2007**, *250*, 294–298.
[31] A. H. Chughtai, N. Ahmad, H. A. Younus, A. Laypkov, F. Verpoort, *Chem. Soc. Rev.* **2015**, *44*, 6804–6849.
[32] A. Corma, H. García, F. Llabrés i Xamena, *Chem. Rev.* **2010**, *110*, 4606–4655.
[33] V. Isaeva, L. Kustov, *Pet. Chem.* **2010**, *50*, 167–180.
[34] Y. Liu, J. Wang, T. Li, Z. Zhao, W. Pang, *Tetrahedron* **2019**, *75*, 130540.
[35] C. Mondelli, G. Gözaydın, N. Yan, J. Pérez-Ramírez, *Chem. Soc. Rev.* **2020**, *49*, 3764–3782.
[36] S. Mitchell, R. Qin, N. Zheng, J. Pérez-Ramírez, *Nat. Nanotechnol.* **2021**, *16*, 129–139.
[37] T. Lunkenbein, J. Schumann, M. Behrens, R. Schlögl, M. G. Willinger, *Angew. Chem.* **2015**, *127*, 4627–4631; *Angew. Chem. Int. Ed.* **2015**, *54*, 4544–4548.
[38] J. Gislason, W. Xia, H. Sellers, *J. Phys. Chem. A.* **2002**, *106*, 767–774.
[39] S. Hock, M. Lucas, M. Rose (Technische Universität Darmstadt), DE 102021103940 A1, **2021**.
[40] D. Duca, G. Barone, Z. Varga, *Catal. Lett.* **2001**, *72*, 17–23.
[41] M. C. Militello, S. J. Simko, *Surf. Sci. Spectra* **1994**, *3*, 387–394.
[42] M. C. Militello, S. J. Simko, *Surf. Sci. Spectra* **1994**, *3*, 395–401.
[43] S. Hock, L. Iser, M. Lucas, M. Rose, *Chem. Ing. Tech.* **2022**, *94*, 1704–1710.
[44] G. H. Major, N. Fairley, P. M. Sherwood, M. R. Linford, J. Terry, V. Fernandez, K. Artyushkova, *J. Vac. Sci. Technol. A: Vacuum, Surfaces, and Films* **2020**, *38*, 061203.
[45] N. Fairley, V. Fernandez, M. Richard-Plouet, C. Guillot-Deudon, J. Walton, E. Smith, D. Flahaut, M. Greiner, M. Biesinger, S. Tougaard, D. Morgan, J. Baltrusaitis, *Appl. Surf. Sci. Adv.* **2021**, *5*, 100112.
[46] M.P Seah, *Surf. Interface Anal.* **2012**, *44*, 1353–1359.
[47] V. Muravev, G. Spezzati, Y.-Q. Su, A. Parastaev, F.-K. Chiang, A. Longo, C. Escudero, N. Kosinov, E. J. Hensen, *Nat. Catal.* **2021**, *4*, 469–478.

Manuscript received: November 28, 2022
Revised manuscript received: March 14, 2023
Accepted manuscript online: March 17, 2023
Version of record online: April 17, 2023